

Scanning Kelvin Force Microscopy For Characterizing Nanostructures in Atmosphere

J. J. Kopanski, M. Y. Afridi, S. Jeliaskov, W. Jiang, and T. R. Walker

*Semiconductor Electronics Division
National Institute of Standards and Technology
100 Bureau Dr., Stop 8120
Gaithersburg, MD 20899*

Abstract. The Electrostatic Force Microscope (EFM) and the related Scanning Kelvin Force Microscope (SKFM) are of interest for the measurement of potential distributions within nanostructures and for work function measurements of gate metals for next generation CMOS. EFM phase mode has better spatial resolution than SKFM because its signal depends on the electric field gradient, while the SKFM's signal depends on the electric field directly. We have determined the effect of data acquisition conditions on spatial resolution and accuracy of CPD measured with SKFM in atmosphere by using various commercially available tips and a specially designed test chip containing up to four different metal layers. The test chip contains structures intended to simulate nanoparticles and nanowires in various combinations of metals. By comparison to measurements on the test structures using tips with known work functions, the effective work functions of tips with unknown work functions can be estimated. A simple computer model was developed that predicts SKFM signal as a function of tip and sample measurement geometries. Qualitative agreement between the measured and modeled SKFM signal is seen.

Keywords: contact potential difference, EFM, electrostatic force microscope, scanning Kelvin force microscope, SKFM, work function.

PACS: 73.22.-f, 73.30.+y, 73.40.Cg, 73.63.-b

INTRODUCTION

Simple and accurate measurement of metal work functions would be useful for multiple applications. Next generation CMOS integrated circuits will require metal gates on top of high-k dielectrics. Candidate gate metals must have complementary work functions for the matched PMOS and NMOS transistor pairs. Emerging beyond CMOS, nanowire devices have similar work function characterization needs.

An attractive method of measuring surface potential is the electrostatic force microscope (EFM) and the related scanning Kelvin force microscope (SKFM) [1]. Both microscopes respond to surface potential and operate similarly, but measure different signals. The EFM in phase mode, conducts two sweeps over the same topography. The first sweep measures surface topography using a tapping mode atomic force microscope (AFM), which depends on a mechanical oscillation of the cantilever. The second sweep is conducted with the tip lifted a constant height above the topography. The measured signal is the phase of the tip oscillation relative to the drive signal,

which is affected by the local surface potential of the sample. The SKFM is also a two sweep technique. The first sweep again measures topography. The second sweep is conducted with the tip lifted above the topography, but in this case the mechanical oscillation of the cantilever is turned off and a dc + ac voltage is applied between the tip and sample at the cantilever oscillation frequency. Any potential difference between the work function of the sample and the work function of the tip generates a force between the tip and sample, resulting in a physical oscillation of the cantilever. The SKFM uses a feedback loop to adjust the dc potential applied to the tip to minimize this force (and oscillation of the cantilever). This dc nulling voltage is a measure of the contact potential difference (CPD) between the tip and sample. CPD is defined as:

$$CPD = \varphi_{tip} - \varphi_{sample} \quad (1)$$

where φ_{tip} is the work function of the tip and φ_{sample} is the work function of the sample.

Both EFM phase mode and SKFM have limitations in spatial resolution, accuracy, and reproducibility of the work function measurement. While EFM phase mode and SKFM are in some ways similar to other proximal probe techniques like AFM and scanning tunneling microscopy (STM), they do not achieve the same type of spatial resolution. This is because the tip-sample interactions which generate the image have different length dependencies. Electron tunneling current, measured by STM, falls off exponentially with probe-sample separation; the van der Waals forces which govern AFM fall off with the inverse sixth power of probe-sample separation [2]. In contrast, the capacitive force associated with the contact potential measured by SKFM falls off as the inverse square of the probe-sample separation. EFM depends on the gradient of the force and has an inverse cubed dependence [3]. In practice, this means that the entire conductive surface of the cantilever probe tip used by SKFM contributes significantly to the measured CPD and sharp transitions in local sample work function are not well resolved. Although EFM has higher spatial resolution, it does not give the CPD directly.

The CPD signal measured by SKFM is extremely sensitive to the surface of the sample. In atmosphere, contamination, surface moisture [4], and oxidation of the sample and the tip can result in changes of the measured CPD. The CPD measured with SKFM of a clean gold surface in atmosphere can be observed to change over a period of several days as contamination builds up on the surface. Hence, SKFM based CPD measurements of even freshly deposited or polished metal surfaces in atmosphere can be expected to vary from the ideal.

At least two other factors also affect the apparent reproducibility of SKFM measurements. Because the tip sidewalls and cantilever contribute to the average CPD signal measured, the exact tip-to-sample geometry can affect the measured CPD for non-uniform samples. Hence a different CPD could be measured as the orientation of a non-uniform sample relative to the cantilever is changed, even if the tip is contacting the sample at the same point. Surface charging can also affect reproducibility. Voltages applied to the SKFM can deposit considerable charge, resulting in a shift of the apparent CPD.

In this work, we have examined the factors that affect the accuracy and reproducibility of EFM phase mode and SKFM measurements in atmosphere. Towards this end, we designed and constructed a test structure capable of containing four separate metals with different work functions. We have also developed a simple computer model capable of predicting the contribution to the measured CPD of the various parts of a cantilevered probe tip when scanned over a sample with non-uniform work function.

Results of SKFM measurements on this test structure and a comparison to model results are presented below.

TEST STRUCTURES

A test chip providing structures with up to four metals with different work functions was designed and fabricated. Metal layer 1 was designed for definition by etching; metal layers 2, 3, and 4 were designed for definition by lift-off lithography. The test chip contains 5 different types of structures: structures to measure the electrical line width; MOS capacitors with guard bands; broken lines of various lengths with 3 μm , 5 μm , or 10 μm width and spacing; metal squares with 3 μm , 5 μm , or 10 μm side length and spacing; and interdigitated electrodes. The interdigitated electrodes have 50 fingers on each side, with finger widths and spacings of 5 μm . These electrodes were designed in all 16 possible combinations of 4 metals, i.e. metal-1-to-metal-1, metal-1-to-metal-2, ..., metal 4-to-metal-3, and metal-4-to-metal-4. An overview image of part of the broken line test structures is included as Figure 1. For the work described here, the structure was fabricated with just 3 of the possible 4 metals. These three metals were aluminum ($\phi_{\text{Al}} = 4.28 \text{ eV}$), chromium ($\phi_{\text{Cr}} = 4.5 \text{ eV}$), and gold ($\phi_{\text{Au}} = 5.1 \text{ eV}$) – which provide a good range of variation in work function. The accepted values for work functions used in this paper are from [5].

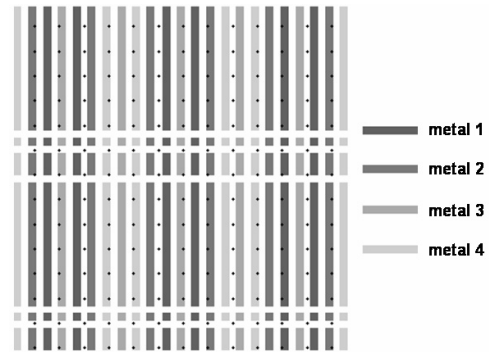


FIGURE 1. Mask design of a series of broken lines in four different metals, depicted here as four different shades of gray. Various repeat patterns of the four metals are available on the test chip to determine the effect of the neighboring lines on the CPD measured at the tip location. Line width and spacing here is 3 μm ; grid dot spacing is 10 μm .

MODEL

A simple one-dimensional (1-D) model of the SKFM was implemented in Visual Basic, based on

models developed in [2, 6, 7, 8]. This model considers the contributions of the hemispherical tip, conical tip shank, and cantilever (broken into rectangular elements) separately through analytical expressions for the capacitances of these elements to a planar sample. Figure 2 shows a graphical representation of this model over an ideal structure. This piecewise approximation works because in SKFM, the first harmonic of the tip force, F_ω , depends on the capacitance between the elements of the tip and the surface and not on capacitances between the different surface elements. Even though this model is inherently 1-D and cannot achieve spatial resolution smaller than the tip radius, it allows an estimate of the measured CPD that includes the contribution of all parts of the probe over complex structures (like the lines of different metals in the test structure).

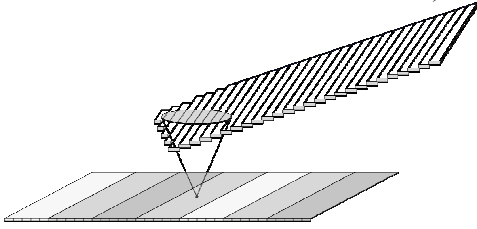


FIGURE 2. Piecewise model of SKFM (not to scale). The three components of the model are the spherical tip, the conical tip sidewall, and the rectangular cantilever. The cantilever is divided into 1 μm segments, each of which is considered individually with respect to the work function of the segment of the sample directly beneath it.

The total force between elements of the tip/cantilever and the surface is given by:

$$F_\omega = \sum_{i=1}^n \frac{dC_i}{dz} (\varphi_i - \varphi_{dc}) U_{ac} \quad (2)$$

where F_ω is the total force acting on the probe at the applied ac voltage frequency, ω ; dC_i/dz is the differential capacitance of the i^{th} element of the probe; φ_i is the work function of the i^{th} element; φ_{dc} is the applied dc bias; and U_{ac} is the applied ac bias. Setting $F_\omega = 0$ and solving for φ_{dc} yields an expression for the applied dc bias needed to minimize the force on the probe:

$$\varphi_{dc} = \frac{\sum_{i=0}^n \left(\frac{dC_i}{dz} \varphi_i \right)}{\sum_{i=0}^n \frac{dC_i}{dz}} \quad (3)$$

Explicitly expressing the contributions of the three elements of the probe yields the equation implemented in the model:

$$\varphi_{dc} = \frac{\frac{dC_{tip}}{dz} \langle \varphi \rangle_{tip} + \frac{dC_{shank}}{dz} \langle \varphi \rangle_{shank} + \sum_{i=0}^n \left(\frac{dC_{i,cantilever}}{dz} \varphi_i \right)}{\frac{dC_{tip}}{dz} + \frac{dC_{shank}}{dz} + \sum_{i=0}^n \frac{dC_{i,cantilever}}{dz}} \quad (4)$$

Comparison of the model with measured SKFM signal will be presented in the next section.

RESULTS

The results of a survey of the apparent work functions of the three metal films on the test structure, as measured by SKFM, are shown in Table 1. These were measured first with a PtIr₅ ($\varphi_{\text{PtIr}} = 4.86$ eV) coated tip and then with a TiPt ($\varphi_{\text{Ti}} = 4.33$ eV) coated tip. Tip lift height was 50 nm. Measurements were performed a long time after device fabrication and should represent the steady state value of the work function of the films in atmosphere. With a clean surface and fresh tip, values relatively close to the accepted clean surface values were obtained with both tips. Of the three metals, Al is the most susceptible to oxidation in atmosphere and displays the largest variation from its clean surface value, about 400 mV.

The data in Table 1 are measured with the cantilever centered over the bonding pad of the interdigitated electrode, which should expose all parts of the tip and cantilever to the target metal. All three metals were measured in rapid succession using the same tip. Prior to imaging, the sample surface was cleaned using transfer tape that was adhered to the surface by partially dissolving it in high purity acetone. Subsequent removal of the tape removed most particulates. This procedure also increased the contrast in the SKFM image. The value reported is an average over a quadrant of the image, approximately 4,000 points. Once a stable image was obtained, the measurement stayed within ± 100 mV for a large number of scans. Uncertainties reported are for CPD extracted from a single image.

The apparent good agreement of the measured work functions with the reference values was not expected. In particular, the measurement was made in ambient atmosphere with a relative humidity of 60%, which has been shown to mask the surface potential leading to less SKFM image contrast [4]. An effect like this is apparent in Fig. 3 and Fig. 5 where the contrast between Al and Au is less than the measurement in Table 1. Multiple factors were seen that affected the value of CPD measured by SKFM. The most important of these were the tip lift height, the phase of the lock-in relative to the drive frequency, contaminants on the sample and tip, and damaged or worn tips. Likewise, a large over voltage applied to the sample could induce large changes in the measured

Metal	work function ref. value (eV)	PtIr ₅ tip		TiPt tip	
		CPD (V)	ϕ (eV)	CPD (V)	ϕ (eV)
Al	4.28	+0.88 ± 0.03	3.98 ± 0.27	+0.45 ± 0.10	3.84 ± 0.22
Cr	4.5	+0.14 ± 0.05	4.76 ± 0.21	-0.40 ± 0.34	4.73 ± 0.39
Au	5.1	-0.18 ± 0.04	5.04 ± 0.20	-0.71 ± 0.22	5.04 ± 0.30

CPD that was persistent, presumably from deposited charge.

The repeatable separation in work functions measured with from these three metals suggests an easy method for estimating the work function of an SKFM tip. By plotting the known work functions of the three metals versus measured CPD, the work function of the tip should correspond to the intercept of the line with the work function axis at CPD = 0.

A line scan of the CPD measured with SKFM for the Al-Au interdigitated electrode as a function of tip-sample lift height is shown in Figure 3. The CPD reaches a constant value in the center of the metal lines, but not in the center of the oxide separator line. A fairly sharp transition is seen in CPD between metal and oxide, though it is obvious that the metal lines are still influencing the measured CPD, even when the SKFM tip is midway between the two lines. Because the tip sidewalls and cantilever contribute to the measured CPD, this mode of SKFM cannot measure an accurate value of CPD of objects smaller than a few micrometers. As tip lift height is increased from 2 nm to 2000 nm the transition between lines grows broader, approaching the average CPD of the surface as the tip lift is made larger.

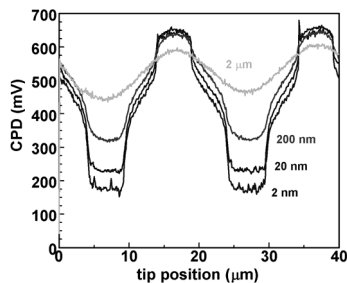


FIGURE 3. SKFM measured CPD of alternating Au and Al lines as a function of tip lift height. The region between lines is silicon covered with 5 nm of silicon dioxide. The measured CPD of each line is affected by the neighboring lines.

Figure 4 shows the results of our model calculation for the same structure using model tip parameters matching the tip used for the measurements, in this

case, a Point Probe Plus EFM tip from Nanosensors.* The tip was modeled with a tip radius, r_{tip} , of 25 nm; a cone angle, CA, of 21°; a tip shaft length, L_{tip} , of 13 μ m; a cantilever length, L_c , of 225 μ m; and a cantilever width, W_c , of 28 μ m. The modeled behavior is similar to the experiment, with the tip dominating the signal at small lift heights, the tip sidewalls dominating at intermediate heights, and the cantilever dominating at large heights. The model can be used to predict the shape of the tip and cantilever for the best spatial resolution. Cantilevers should be narrow, while the tip sidewalls should be long and steep. Extremely sharp tips may not have the best spatial resolution if the capacitance of the tip sidewall is sufficient to overwhelm the capacitance due to the tip. A slightly blunt tip, relative to the sidewall area is required.

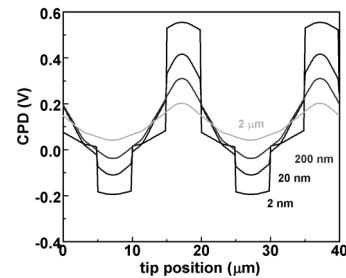


FIGURE 4. Model results of the structure experimentally imaged in Fig. 3.

Figure 5 shows a comparison of CPD measured with SKFM to the EFM phase signal. The EFM signal shows noticeably greater spatial resolution. Although SKFM gives a direct measurement of CPD, its spatial resolution is poor because all parts of the cantilever contribute to the signal. The EFM-phase mode is based on the measurement of the force gradient rather than the force itself.

Since they are sensitive to the same sample parameter, the question arises: Can the spatial resolution of the EFM-phase mode be combined with the quantitative measurement of CPD of the SKFM?

* Certain commercial equipment, instruments, or materials are identified in this paper in order to adequately specify the experimental procedure. Such identification does not imply recommendation or endorsement by NIST, nor does it imply that they are necessarily the best available for the purpose.

Figure 6 shows measurement of EFM phase as a function of applied dc bias. For CPD measured with SKFM, an applied dc bias shifts the measured CPD voltage by the same amount. The behavior of the EFM phase is more complex. The magnitude of phase increases the larger the dc voltage is compared to the CPD; with the peak (minimum phase magnitude) in the vicinity of where the applied dc bias equals the opposite of the CPD [9]. This data was acquired over the range of +10 V to -10 V, which resulted in some shifting of the surface potential due to deposited charge.

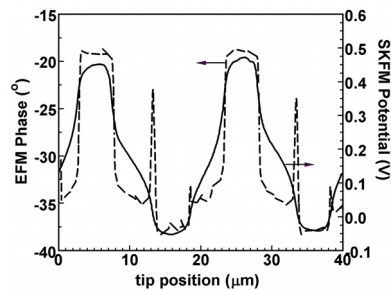


FIGURE 5. CPD measured with SKFM (solid line) and phase measured with EFM (dashed line) of the alternating Au and Al lines of the test structure.

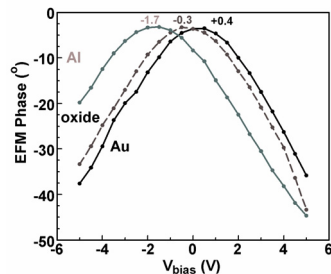


FIGURE 6. EFM phase versus dc bias of the Al (gray, peak at -1.7 V), oxide (dashed, -0.3 V), and Au (black, +0.4 V) regions of the test structure. Data were acquired in 0.5 V steps from -10 V to +10 V by applying each voltage for 1/40 of the time to acquire the image. The average phase was then extracted from the corresponding fraction of the image.

Multiple extensions of the Kelvin force technique have been suggested using high-Q cantilevers operating in ultra-high vacuum, notably the frequency demodulated Kelvin probe [10 - 11]. In future work, we will explore the dependence of EFM phase on local CPD with high-Q cantilevers in atmosphere.

CONCLUSIONS

Measurements of the work functions of some common metals in atmosphere with the SKFM were found to be related to their clean surface values [5]. Despite problems with determining absolute values of work function, the authors feel that SKFM and EFM

phase mode measurements can still be important characterization tools because they can detect relative differences in work function. Careful control of sample cleanliness, attention to the tip condition, SKFM operating conditions, and use of known references are needed to assure a reproducible measurement. The effects of the capacitive coupling of the tip sidewalls and cantilever to the sample are seen in measurements across abrupt boundaries, and the magnitude of the effect has been reproduced in a simple 2-D model. This means that while the SKFM in atmosphere can measure a meaningful work function value of large area samples, the work function of small area samples (such as nanowires) cannot be separated from the effects of the work function of the surrounding matrix. EFM phase mode displays higher spatial resolution than SKFM, though it does not provide a direct measurement of work function. The test structure and modeling capability presented here are useful tools to evaluate future improvements in the SKFM technique.

ACKNOWLEDGMENTS

Thomas Walker participated in this work through a NIST Summer Undergraduate Research Fellowship, supported in part by the National Science Foundation under grant No. #0139217. This work was performed in part at the Center for Nanoscale Science and Technology Nanofab at the National Institute of Standards and Technology.

REFERENCES

1. M. Nonenmacher, M. P. O'Boyle, and H. K. Wickramasinghe, *Appl. Phys. Lett.* **58**, 2921-2923 (1991).
2. M. Saint Jean, S. Hudlet, C. Guthmann, and J. Berger, *J. Appl. Phys.* **86**, 5245-5248 (1999).
3. J. Colchero, A. Gil, and A. M. Baró, *Phys. Rev. B* **64**, 245403 (2001).
4. H. Sugimura, Y. Ishida, K. Hayashi, O. Takai, and N. Nakagiri, *Appl. Phys. Lett.* **80**, 1459-1461 (2002).
5. H. B. Michaelson, *J. Appl. Phys.* **48**, 4729-4733 (1977).
6. H. O. Jacobs, P. Leuchtman, O. J. Homan, and A. Stemmer, *J. Appl. Phys.* **84**, 1168-1173 (1998).
7. G. Koley, M. G. Spencer, and H. R. Bhangale, *Appl. Phys. Lett.* **79**, 545-547 (2001).
8. A. Gil, J. Colchero, J. Gómez-Herrero, and A. M. Baró, *Nanotechnology* **14**, 332-340 (2003).
9. C. H. Lei, A. Das, M. Elliott, and J. E. Macdonald, *Nanotechnology* **15**, 627-634 (2004).
10. U. Zerweck, C. Loppacher, T. Otto, S. Grafström, and L. M. Eng, *Phys. Rev. B* **71**, 125424 (2005).
11. C. Loppacher, U. Zerweck, S. Teich, E. Beyreuther, T. Otto, S. Grafström, and L. M. Eng, *Nanotechnology* **16**, S1-S6 (2005).